Microtubule Response to Tensile Stress Is Curbed by NEK6 to Buffer Growth Variation in the Arabidopsis Hypocotyl

Shogo Takatani, Stéphane Verger, Takashi Okamoto, Taku Takahashi, Olivier Hamant, Hiroyasu Motose

Microtubule response to tensile stress is curbed by NEK6 to buffer growth variation in the Arabidopsis hypocotyl

Shogo Takatani[1,2], Stéphane Verger[2,3], Takashi Okamoto[1], Taku Takahashi[1], Olivier Hamant[2]*, Hiroyasu Motose[1]*

1. Department of Biological Science, Graduate School of Natural Science and Technology, Okayama University, 3-1-1 Tsushimanaka, Okayama, 700-8530, Japan.
2. Laboratoire de Reproduction et Développement des Plantes, Université de Lyon, ENS de Lyon, UCB Lyon 1, CNRS, INRAE, F-69007 Lyon, France
3. Present address : Umeå Plant Science Centre, Department of Forest Genetics and Plant Physiology, Swedish University of Agricultural Sciences, SE-901 83 Umeå, Sweden

Correspondence : olivier.hamant@ens-lyon.fr, motose@cc.okayama-u.ac.jp
Lead contact: Olivier Hamant olivier.hamant@ens-lyon.fr

Summary

Growth variability generates mechanical conflicts in tissues. In plants, cortical microtubules usually align with maximal tensile stress direction, thereby mechanically reinforcing cell walls, and channeling growth rate and direction. How this is achieved remains largely unknown and likely involves microtubule regulators. The NIMA-related microtubule-associated kinase NEK6 phosphorylates tubulin, leading to the depolymerization of a subset of microtubules. We found that cortical microtubules exhibit a hyper-response to mechanical stress in the *nek6* mutant. This response contributes to local cell protrusions in slow growing regions of the *nek6* mutant hypocotyl. When growth amplitude is higher, the hyper alignment of microtubules leads to variable, stop-and-go, phenotypes, resulting in wavy hypocotyl shapes. After gravistimulation or touch, the *nek6* mutant also exhibits a hyperbent hypocotyl phenotype, consistent with an enhanced perception of its own deformation. Strikingly, we find that NEK6 exhibits a novel form of polarity, being recruited at the ends of a subset of microtubules at cell edges. This pattern can be modified after local ablation, matching the new maximal tensile stress directions. We propose that NEK6 depolymerizes cortical microtubules that best align with maximal tensile stress to generate a noisier network of microtubules. This

prevents an over-reaction of microtubules to growth variations, and instead, promotes the buffering of growth variations.

Keywords: Microtubule, mechanical stress, morphogenesis, variability, suboptimality, growth, Arabidopsis

Introduction

Robustness in living organisms emerges from coupling intrinsically suboptimal processes, be it at molecular scales, at the level of gene regulatory networks (e.g. [1]) or of cell/cell interactions. The contribution of mechanical forces to plant organ morphogenesis is important, and mechanics has been proposed to add robustness to cell functions, yet whether mechanical cues are optimally perceived at cell and organ scale is not known.

Mechanical forces have been proposed to add robustness to cell functions, notably by providing synchronizing cues for adjacent cells and constraining molecular outputs [2][3]. Because plant cells do not migrate, final organ shape is a good proxy for robustness at multiple scales, notably integrating the contribution of mechanical signals from molecules to multicellular forms. More specifically, the mechanics behind cell shapes mainly rely on cell walls, and within the cell wall, cellulose microfibrils appear as the main load-bearing components [4]. Because cortical microtubules (CMTs) usually guide the deposition of cellulose in cell walls, CMT behavior is a good proxy for final plant cell and tissue shapes. Last, cell walls are constantly under high tensile stress, being pulled by turgor pressure in the MPa range. Interestingly, CMTs have been shown to align with maximal tensile stress direction in most aerial plant organs [5][6][7][8][9]. This response has been involved in the maintenance of cell shapes [7][10], in monitoring growth heterogeneity [11][12] and in restricting organ growth [13]. The CMT – plant shape nexus is thus key to shape robustness. Here we observed that mutation in a microtubule kinase confers hyper alignment of microtubules, and we relate this behavior to mechanical stress and growth.

Many Arabidopsis mutants impaired in microtubule dynamics exhibit shape defects. This is notably the case of the katanin mutant which exhibits reduced microtubule self-organization abilities, due to reduced severing frequency, and thus a reduced response of microtubules to mechanical stress [14][11]. These defects result in the formation of isotropic CMT arrays in most cells, isotropic growth, and impaired organ elongation. The Arabidopsis NIMA (Never In Mitosis A)-related kinase 6 (NEK6) is also involved in directional cell elongation through its impact on microtubule organization [15][16][17][18]. NEK6 kinase activity and localization on microtubules are essential for cell elongation [15]. Cortical microtubules in *nek6* mutant are resistant to microtubule depolymerization drugs, suggesting that NEK6 destabilizes cortical microtubules [16]. NEK6-mediated β-tubulin phosphorylation prevents

polymerization of aberrant microtubules, suggesting that NEK6 depolymerizes specific types of cortical microtubules [17]. A recent study in the basal land plant *Marchantia polymorpha* further demonstrates the evolutionarily conserved NEK-dependent mechanism of directional cell growth through microtubule depolymerization [19]. The biochemical characterization of NEK6 thus offers the unique opportunity to investigate the contribution of microtubule polymerization rate in the microtubule response to stress. The possibility to modify microtubule dynamics in a novel way could also help us identify new functions, and possibly an optimum, for the microtubule response to stress. Here, through mechanical perturbation and live imaging, we show that NEK6 reduces the microtubule response to stress; this also reduces proprioception, thereby smoothing tissue and cell growth patterns in the hypocotyl.

Results

nek6-1 mutants exhibit wavy and stop-and-go growth patterns in the fast-growing region of the hypocotyl

Previously, we reported that *NEK6* is required for both directional cell growth and organ development ([20], Figure 1A and 1B, Figure S1F and S1G). To investigate precisely the organ-scale defect of *nek6-1* mutant, seedling growth was recorded over time (Figure 1A and 1B, Video S1). The wild type exhibited slight fluctuations in its growth trajectory; in contrast, the *nek6-1* mutant displayed marked growth deviations: the *nek6-1* hypocotyls did not grow straight (Figure S1B, N_{WT}=74, N_{nek6}=80, *p*-value=4.0x10^{-9} *t*-test). This waving phenotype was mostly restricted to the rootward region of the hypocotyl, i.e. in the lower half of the hypocotyl ([9], Figure 1A and 1B). As reported before, we could also observe ectopic outgrowth of epidermal cells [15][18]. Interestingly, these were instead mainly located in the shootward region of the hypocotyl (Figure S1A).

To quantify this phenotype, we defined waviness as the ratio between hypocotyl length and the shortest, straight, distance between seed and cotyledon (Figure 1C). The hypocotyl exhibits a well established and stereotypical growth gradient, where rootward cells are growing much faster than shootward cells [21][9]. Differences in growth defects along the *nek6* hypocotyl may be due to such prepattern. To test that hypothesis, we first correlated hypocotyl length and waviness in *nek6*. 7-day old seedlings differ in hypocotyl length even

within the same line and such natural variation was large enough to draw a correlation. We found that shorter hypocotyls were less wavy. On the contrary, longer hypocotyls were wavier (Figure 1C; Pearson's correlation, n_{WT}=53 r=0.34, *p*-value =0.013, $n_{nek6\text{-}1}$=64, r=0.55, *p*-value=2.5 x 10^{-6}). As cell divisions are rare in hypocotyls[21], this shows that, in *nek6*, wavy growth correlates with rapid cell elongation.

Next we counted the number of ectopic outgrowth in shootward (upper half) and rootward (lower half) of hypocotyl using a previously reported method [15]. This analysis confirmed that the number of ectopic outgrowth is increased in the shootward region of the hypocotyl, where cell growth is reported slower (Figure S1C). In contrast to hypocotyl waviness, the presence of ectopic outgrowths correlates with slower growth.

To further test this correlation, we stimulated hypocotyl elongation by growing seedlings in the dark. In these conditions, wild-type and *nek6-1* seedlings exhibited growth deviations throughout the length of their hypocotyls (Figure S1D and S1E). Interestingly, ectopic outgrowth was completely suppressed in dark-grown *nek6-1* mutant (Figure S1E). This further confirms that ectopic outgrowth and hypocotyl waviness correlate with slow growth and fast growth, respectively.

nek6 mutation amplifies hypocotyl growth deviations after gravistimulation or touch

Next, we tested whether the *nek6* mutation induces or amplifies a pre-existing wavy growth pattern. To do so, we imposed external constraints on hypocotyl growth.

First, we gravistimulated young *nek6-1* seedlings. We reasoned that if the *nek6* mutation induces wavy growth independent of the hypocotyl's normal growth pattern, the response of the hypocotyl to gravity in *nek6* should be noisier, whereas, if the *nek6* mutation amplifies the wild-type response to gravity, the *nek6* hypocotyls should be more curved than the wild type. Seedlings were grown on agar medium in the dark and rotated by 90 degrees from the original orientation to induce gravistimulation (Figure 1D). After gravistimulation, seedlings grew upward against gravity in both the wild type and *nek6-1* mutant 3 hours after gravistimulation. However, *nek6-1* mutant seedlings displayed more curvy hypocotyls 16 hours after gravistimulation, when compared to the wild type (Figure 1D). The difference between wild-type and mutant waviness was significant (n_{WT}=12, $n_{nek6\text{-}1}$=13, *p*-value =0.026 Mann-Whitney

U-test). Some *nek6-1* mutant hypocotyls were even curved at an angle superior to 90 degrees (Figure 1E). Note that the *nek6-1* mutant could respond to gravity as quickly as the wild type (Figure S1H, n_{WT}=10, n_{nek6-1}=7, n.s. *p*-value>0.05 *t*-test). Thus the *nek6-1* mutant is not agravitropic, but it exhibits a specific defect in growth direction rather than gravitropism.

To further confirm that the *nek6-1* mutant amplifies wild-type growth patterns, we exposed *nek6-1* seedling to a touch stimulus. When slanting plates, roots touch the medium as they grow and this modifies their trajectory (e.g. [22]). We performed the same test for dark-grown hypocotyls. Agar medium containing plates were inclined forward with an angle of 30 degrees to induce upward bending growth of hypocotyls and continuous mechanical friction between seedlings and agar medium (Figure 1F and 1G). In these conditions, wild-type hypocotyl growth was slightly skewed, whereas *nek6-1* hypocotyls were very curvy, sometimes even exhibiting a full loop phenotype (Figure 1I). Wild type and mutant exhibited significant difference in their waviness (Vertical: n_{WT}=19, n_{nek6-1}=19 *p*-value=5.7×10^{-11}, Oblique: n_{WT}=22, n_{nek6-1}=23, *p*-value=7.1×10^{-6} Mann-Whitney *U*-test). Altogether, these observations support a scenario in which growth deviations are amplified in the *nek6* mutant.

Microtubules are hyper-aligned along the longitudinal axis of *nek6* hypocotyls in the fast-growing region

Because of the biochemical function of NEK6 as a tubulin kinase and knowing that cortical microtubules are major regulators of growth direction, we next checked the microtubule organization in the basal region of *nek6* hypocotyls. In the wild type, CMTs display rotating or unstable organizations in the fast growing region of the hypocotyl [23][24], and they become predominantly longitudinal later on as growth slows down [25][26][27]. To quantify CMT behavior in hypocotyl cells, we used the ImageJ macro FibrilTool, which is based on the concept of nematic tensors and measures the average orientation and anisotropy of CMT arrays [28]. All numbers in this article relate to microtubule orientation and anisotropy per cell. The *nek6-1* mutant exhibited more consistent CMT orientations than the wild type, especially in the rootward part of the hypocotyl (Figure S2). Overall, the standard deviation of CMT orientation was smaller in *nek6-1* than in the wild type (Figure S2E, n_{WT}=13, n_{nek6-1}=11, *p*-value=0.033 *t*-test).

Observation of the same cells over two hours confirmed that CMTs in the wild type continuously change their orientation (Figure 2A). Although we could detect a bias towards the longitudinal axis when averaging CMT orientations, microtubule arrays in the wild type could completely change their orientation in only one hour (Figure 2B). In contrast, most CMTs aligned longitudinally in the *nek6-1* mutant (Figure 2B, Figure S2) and CMT reorientations were dramatically reduced (Figure 2C). When pooling the quantifications together, we found that the reorientation angle of CMTs in 1 hour was significantly smaller in *nek6* than in the wild type (Figure 2D, n_{WT}=136, $n_{nek6\text{-}1}$=128 *p*-value=1.5x10^{-8} Mann-Whitney *U*-test). Therefore, the *nek6* mutation seems to reduce the deviations in CMT behavior in the fast growing region of the hypocotyl. Altogether, our data suggest that, in the *nek6* mutant, the CMT pattern is denoised and this amplifies the hypocotyl response to growth fluctuations.

The microtubule response to mechanical perturbations is increased in *nek6*

The presence of longitudinal microtubules after a fast growing phase in hypocotyls has been related to the pattern of tensile stress in the hypocotyl epidermis: the inner tissues would pull the epidermis along the axis of the hypocotyl, and the epidermis would resist by aligning CMTs (and reinforcing its outer walls) in the longitudinal direction [8]. Such stress pattern and CMT alignment have been further validated using mutants with cell-cell adhesion defects [9]. Given the hyper-alignment of longitudinal CMTs, and the overall hyper-response to growth fluctuations in *nek6* (Figure S2), we next investigated whether CMTs in *nek6* could be more sensitive to tensile stress than the wild type.

To check this, we locally changed the stress pattern in hypocotyls by performing cell ablations. Because the epidermis is under tension, the pattern of stress becomes circumferential around the ablation site, and CMT orientation follow this pattern within 2 hours [6][8][9]. We confirmed this response in the wild type and observed that the response was more pronounced in the *nek6-1* mutant, at least qualitatively (Figure 3A). We then quantified the anisotropy and average angle of the CMT arrays using FibrilTool, using the method described in [9] (Figure 3B and 3D, [28]). We found that CMT array anisotropy is significantly increased in the *nek6-1* mutant (Figure 3B, n_{WT}=164, $n_{nek6\text{-}1}$=93, *p*-value$_{0.5h}$=4.7x10^{-4}, *p*-value$_{2.5h}$=1.4x10^{-7} *t*-test) and that CMT arrays around the ablation are significantly more circumferential in the mutant than in the wild type (Figure 3D n_{WT}=164, $n_{nek6\text{-}1}$=93, *p*-value=0.049 test Kolmogorov-Smirnov test).

Four hours after ablation, wild-type cells surrounding the ablation site already elongated toward the ablation site, matching the CMT orientation and acting as a wound healing mechanism (Figure S3). The reduction in hole area following wound closure was significantly different between WT and *nek6-1* (Figure S3B, n_{WT}=10, $n_{nek6\text{-}1}$=17, p-value$_{2.5h}$=0.042, p-value$_{4.5h}$=0.0024). Here again, cell elongation in *nek6-1* was more pronounced and wound healing was complete earlier than in the wild type (Figure S3).

Note that, in *nek6*, the rapid reorientation of CMTs after ablation may appear contradictory with the stable CMT orientation in the hypocotyl (Figure 1). This is in fact consistent with the idea that CMT response to stress is more pronounced in *nek6*: in the hypocotyl, epidermal cells are continuously pulled by inner cells, whereas after ablation, the stress pattern changes very rapidly. In other words, both sets of observations independently reflect a similar enhanced CMT response to stress in *nek6*. Altogether, these results further confirm that growth responses are amplified in *nek6* and suggest that this behavior is linked to a hyper response of microtubules to mechanical stress in *nek6*.

In the *nek6* mutant, CMTs follow cell shape-derived stress pattern in slow growing region

If our hypothesis is true, a hyper response to mechanical stress should also be consistent with the presence of ectopic outgrowth in the slow-growing shootward region of the hypocotyl in *nek6*. In contrast to the fast growing region of the hypocotyl, and as previously reported [17], CMTs appeared quite disorganized in the slow growing region of the hypocotyl, both in the wild type and in *nek6* (Figure 4A). However, we could detect a bias towards subcellular circumferential CMT organization in *nek6-1* cells (Figure 4A). Cells with circumferential CMTs were often seen in slow growing shootward region where cell curvature is stronger (Figure 4B, n_{WT}=178, $n_{nek6\text{-}1}$=165). To quantify this phenotype, we set the boundary at cell position #8 (see Figure S2A), and counted the number of cells with circumferential CMTs in *nek6*. In the rootward region (cell position #1 to #8), 9 out of 80 cells exhibited circumferential CMTs. In contrast, in the shootward region (cell position #9 to #20), 23 out of 85 cells exhibited circumferential CMTs (Figure S4E, n_{WT}=178, $n_{nek6\text{-}1}$=165).

Assuming that the outer wall is under tension, in the most parsimonious scenario, the convex curvature of the wall would be enough to prescribe a circumferential stress pattern in the bump. Such patterns of tensile stress have been predicted for small group of cells forming an multicellular bump around stomata, with matching circumferential CMTs [7]. This stress pattern has also been modeled in individual bumpy cells, in charophytes and during root hair emergence in Arabidopsis [5][29]. Circumferential CMTs have actually been observed in giant bumpy cells recovering from oryzalin-induced microtubule depolymerization (see Figure S1B in [30]). To quantify this phenotype, we defined the top wall angle as the angle formed by the cone that best fits the outer wall of epidermal cells (Figure S4C). Using this shape descriptor, we could formally show that the most pointy cells, with a top wall angle of about 80°, exhibited circumferential CMTs, while the flatter cells, with a top wall angle of about 120°, did not exhibit such a pattern (Figure S4B-D). Thus, the CMT pattern in the ectopic outgrowths in *nek6* matches the predicted tensile stress pattern.

To examine how circumferential pattern of cortical microtubules is initiated in the *nek6-1* mutant, CMTs in the *nek6-1* hypocotyls were observed over time before the onset of ectopic outgrowth. From dynamic microtubule organization prior to ectopic outgrowth, CMT orientation became gradually circumferential within 1-2 hours (Figure S4F). This is consistent with a scenario in which the curvature of the outer wall prescribes a stress pattern that is anisotropic enough to bias CMT orientation in the *nek6* mutant, but not in the wild type.

If true, after microtubule depolymerization, newly synthesized CMTs should align circumferentially within the bump of these cells. *nek6-1* seedlings were treated with oryzalin for three hours to completely disrupt microtubules and then oryzalin was washed out to repolymerize microtubules. Before oryzalin treatment, microtubules formed a circumferential pattern below the bumpy outer wall (Figure 4C). Cortical microtubules were completely disrupted immediately after oryzalin washout and were still depolymerized 21 hours later. CMTs eventually regenerated to form a circumferential pattern 72 hours after washout (Figure 4C). Thus, without preexisting microtubules, new CMTs can polymerize into the circumferential pattern de novo.

At this stage, we however cannot completely exclude another scenario to explain this CMT pattern: in *nek6*, CMTs may be more sensitive to steric constraints, independent of mechanical stress in the wall. Typically, CMTs may minimize their bending energy, and thus align so as to

be as straight as possible. To test that hypothesis, we observed CMT behavior when mechanical stress magnitude in the wall is increased or reduced. *nek6-1* seedlings were transferred into pure water (increasing tensile stress level in outer walls) or into 0.2 M mannitol solution (reducing tensile stress level in outer walls). CMTs were then observed over time by confocal microscopy. CMT arrays were more circumferential in water-treated seedlings, and this pattern largely disappeared in mannitol-treated seedlings within 1 hour, both in the seedlings before protrusion (2-day old: Figure 4D-G) and after protrusion (3-day old: Figure S4G). As cell shapes were not dramatically impaired by these treatments, at least within a 1-hour window, the circumferential CMT orientation in *nek6* better matches a response to shape-derived stress in the wall, rather than a direct response to cell geometry.

The NEK6 protein exhibits a bipolar localization, with a bias on longitudinal microtubules, in young hypocotyls

Mechanistically, NEK6 has been shown to prevent tubulin polymerization [17]. However, if the polymerization of all microtubules was enhanced in *nek6*, this may not necessarily lead to a hyper response to mechanical stress, or at least to an enhanced directional effect on CMT organization and cell growth. To investigate further how NEK6 affects microtubules, we next analyzed the localization and dynamics of the NEK6 protein in hypocotyls from young seedlings. We used a *geNEK6-GFP* construct (genomic *NEK6* promoter, *NEK6* coding region fused with GFP), which is able to complement the mutant [17]) and introgressed it in the *pUBQ10::mCherry-TUB6* line. NEK6-positive CMTs behaved quite differently than NEK6-negative ones, with significantly more shrinking (Figure 5J, n_{NEK6+}=153, n_{NEK6-}=193, *p*-value =$2.2x10^{-16}$ Fisher's exact test). We however could not detect a significant difference in velocity (Figure S5G, n_{NEK6+}=50, n_{NEK6-}=17, *p*-value =0.92 *t*-test).

Strikingly, we observed that NEK6 exhibits a multipolar localization in the cell, while being recruited on microtubules (Figure 5A). In the bottom half of the hypocotyl, this generated stereotypical patterns with NEK6 being predominantly localized at the apical and basal part of the cell (Figure 5A). NEK6 was not recruited on all microtubules. Instead, by correlating CMT orientation and NEK6-GFP signal, we could detect a bias towards a recruitment of NEK6 on longitudinal CMTs (Figure 5B, 5C and 5E). We plotted NEK6 signal intensity vs. microtubule orientation (Figure 5D). The average NEK6-GFP signal intensity on longitudinal

CMTs was significantly different from NEK6 signal intensity on oblique CMTs (Fig. S5A, n=32 cells from 4 hypocotyls, *p*-value =4.1x10^{-8} *t*-test).

Interestingly, this also corresponds to CMTs that are best aligned with tensile stress. We then performed time-lapse experiments to analyze the dynamics of microtubules and correlate it with the presence of NEK6. We found that NEK6-positive microtubules at basal and apical domains were preferentially depolymerizing (Figure 5F-I, Figure S5, Video S2 and S3), consistent with the biochemical function of NEK6, and further suggesting that NEK6 preferentially depolymerizes longitudinal microtubules in young hypocotyls.

NEK6 preferentially localizes on microtubules that align with maximal tensile stress

Because longitudinal microtubules in the rootward part of the hypocotyl are aligned with growth-induced stress, this suggests that NEK6 preferentially depolymerizes microtubules that are aligned with maximal tensile stress. If true, we should be able to see a relocalization of NEK6 when the stress pattern is modified, independent of cell geometry. To check this, we next performed cell ablations in hypocotyls, as described above, and analyzed the response of CMTs and NEK6. NEK6 localization changed its orientation within 160 minutes, matching the circumferential orientation of CMTs (Figure 6A and 6B). In our kinetics, we could not clearly detect a sequential response: both CMT orientation and NEK6 relocalization after ablation seemed to occur at the same time (Figure S6B). Interestingly, we observed that the NEK6 pattern better matched the tensile stress pattern than CMTs (Figure 6B, Figure S6). In particular, whereas CMTs were still present along all anticlinal walls 160 minutes after ablations, NEK6 exhibited a clear polar localization, with an enrichment on the anticlinal walls closer to the ablation site (Figure 6B). The average NEK6-GFP signal intensity on proximal side of cells adjacent to ablations was significantly higher than on the distal side (Figure 6C and 6D, n=130 from 23 cells of 5 hypocotyls, Pearson's correlation, r=0.36, *p*-value =2.4x10^{-5}).

Altogether, this suggests that NEK6 is preferentially recruited on CMTs that are aligned with maximal tensile stress. This leads to their depolymerization, reducing the microtubule response to stress. Incidentally, this also suggests that the microtubule response to stress is not maximal in the wild type, in a typical suboptimal scenario. Conversely, the *nek6* phenotype

highlights the defects that are triggered by a too efficient response to mechanical stress, namely a hyper response to the cell and tissue own growth.

Discussion

The *nek6* mutant is hyper proprioceptive

There is little doubt that the cytoskeleton is under mechanical control. In animals, acto-myosin is a prominent target of mechanical stress (e.g. [31][32]), with many important morphogenetic consequences (e.g. [33][34][35][36]). In plants, because of the central role of cellulose microfibrils in shaping cells and tissues, the alignment and bundling of cortical microtubule in response to tensile stress plays a role conceptually analogous to actin cables in response to stress in animals to channel growth and shape [37]. Given the absence of cell movement and the rather mechanically dominant role of cellulose microfibrils in cell walls, any defect in microtubule behavior would translate into abnormal organ shapes in plants. This unique property allowed us to check how a hyper-response to stress can be generated and what types of phenotypes are induced. Focusing on the hypocotyl in the *nek6* mutant, we found that cells become more sensitive to their own growth and shape, leading to stop-and-go wavy hypocotyls when growth-derived stress dominates, and epidermal outgrowth when shape-derived stress dominates. In other words, this corresponds to a form of hyper proprioception [3]. There is indeed evidence that plants, like animals, are able to sense their own geometry through the perception of mechanical force patterns. For instance, the perception of stem curvature may dampen the oscillation of growth following gravistimulation [38]. Our analysis of NEK6 provides a multiscale mechanism, from tubulin phosphorylation up to straight hypocotyls, while including the mechanical status of the tissue (Figure 6E). Our work also brings a new light to previous studies showing how microtubules respond differentially to stem bending [39][40][41]. The interplay between actomyosin and microtubule opens another exciting prospect for future research, potentially providing more inter kingdom comparisons to elucidate how mechanical stress contributes to proprioception and morphogenesis.

NEK6 exhibits a unique bipolar microtubule-associated localization

We found that NEK6 preferentially localizes on the longitudinal microtubules at the top and bottom of epidermal cells in young hypocotyls. Our data suggest that this unique pattern is the result of microtubule-dependent NEK6 activity and mechanical stress pattern. Although the corresponding mechanism is unknown, one can explore some hypotheses. In a recent perspective article, we proposed that proteins such as CLASP or MOR1 may recognize the bent shape of microtubule ends for their recruitment, and that tension within the polymerizing microtubule might affect such bending [42]. Given that NEK6 is also recruited at microtubule ends, this may be a possible mechanism for that protein too. Alternatively, NEK6 may be preferentially recruited on microtubule domains with damages (the number of which would be enhanced upon stress), in a way similar to Katanin, which also preferentially targets defects in the microtubule lattice [43].

One could object that such localization may instead depend on cell geometry, independent of mechanical stress. In fact, in *nek6*, microtubules may be longer on average, leading them to become more sensitive to cell geometry; in turn, microtubules that would be "too long" in the wild type would be depolymerized by NEK6. This alternative scenario does not fit our data. We showed that CMTs become circumferential in the bumpy slow growing epidermal cells, only when turgor pressure is high, i.e. when tensile stress is high and directional. As cell geometry does not exhibit any dramatic changes when turgor level is modulated, it would be difficult to explain why cell geometry sensing could also be turgor-dependent without involving mechanical stress in the wall. Furthermore, we observe that NEK6 becomes more circumferential around local ablations in the wild type. After an ablation, the surrounding cells immediately bulge into the dead cell, as the anticlinal wall in the ablated cell is not supported by turgor pressure anymore. If NEK6 was to depolymerize the longer microtubules, such immediate cell deformation would likely trigger a rapid relocalization of NEK6 along the longer, radial, microtubules. Instead, we observe the recruitment of NEK6 on transverse CMTs. Incidentally, this also shows that NEK6 can be recruited on longitudinal or transverse CMTs, further supporting the idea that cell geometry alone is not a good prescriptor for NEK6 localization.

NEK6 reduces the microtubule response to mechanical stress

NEK6 localizes on microtubules in a circumferential pattern around ablation sites and time-lapse imaging showed that NEK6 localizes on the depolymerizing ends of microtubules,

which shrink from edge to center. These NEK6 behaviors are consistent with our hypothesis that NEK6 depolymerizes microtubules that best align with maximal tensile stress direction.

Our work shed a new light on previously published work. First, the correlation between reduced hypocotyl growth rate, CMT behavior and ectopic outgrowth are consistent with previous work. In particular, propyzamide suppresses and taxol enhances protuberance formation in *nek6* mutants [16]. Similarly, treatment with the ethylene precursor ACC shortens seedlings and dramatically increases the number of protuberances [15]. Note that two ingredients are required to generate protrusions: slow growth, for CMTs to align with shape-derived stress, and weaker outer walls. For instance, when CMTs are depolymerized upon ABA treatment, walls should become weaker, promoting the formation of protrusions [44]. In a control situation, protrusions are repressed, not only because CMTs indirectly reinforce the cell wall, but also because CMTs do not reinforce the cell wall in a circumferential way. Altogether this opens the possibility that the impact of hormones on CMTs may be, at least in part, mediated by mechanical stress [42][45].

Several studies in young hypocotyl reported that cortical microtubules exhibit bipolar array, in which microtubule plus ends go near the apical and basal edges of the cell [23][46][47]. The bipolar arrays change their orientations continuously. Given that NEK6 localizes to the microtubule plus ends at the apical and basal cell edges and that longitudinal CMTs are more frequent in the *nek6* mutant, NEK6 most likely depolymerizes longitudinal microtubules in growing hypocotyl (i.e. that are aligned with maximal tensile stress) to promote microtubule rotation in that tissue.

CLASP localizes to cell edges to allow cortical microtubules to overcome sharp edge [48]. Computational simulation demonstrated that the imposed promotion of microtubule trajectory at the apical and basal cell edges increases the number of longitudinal microtubules [48]. As we see this type of response in the *nek6* mutant, it is possible that NEK6 hinders the passage of microtubules at the apical and basal cell edge simply through depolymerization. Microtubules sometimes buckle after reaching sharp edges [48]. As NEK6 localizes to buckling microtubules and as both the length and duration of buckling microtubule is prolonged in *nek6-1* mutant [17], NEK6 might also recognize bending microtubules at the sharp edges. Incidentally, this opens some prospects to explain how microtubules would align with maximal tensile stress: one may propose that defects in the microtubule lattice, either

because they are pulled by tension, or because they buckle, may act as a code for depolymerization. In fact, such defects have been shown to promote the recruitment of Katanin [43], which itself, promotes the microtubule's response to stress in plants [11]. It is also possible that microtubules first respond to mechanical stress and that NEK6 localizes on stable microtubules independently from mechanical stress; this indirect response of NEK6 to stress would be sufficient to curb microtubule accumulation along maximal tensile stress direction.

In addition to NEK6 and CLASP which are both related to microtubule ends, the SPIRAL2 microtubule associated protein has been shown to bind and stabilize the microtubule minus ends in hypocotyls [49][50]. Interestingly, CMTs in *spr2* mutants also exhibit a more pronounced response to mechanical stress, albeit to a much lower degree than in *nek6* [13]. Arguably, this may be due to the rather ambivalent role of SPR2 as the corresponding mutant exhibits a reduction in catastrophe rate at the microtubule plus end and an increase in depolymerisation rate at the microtubule minus end [50], with different impacts on severing rate depending on the tissue [51][49][50].

A conserved role of NIMA-related kinases in other kingdoms?

NIMA-related kinases (NEKs) in fungi and animals mainly regulate mitotic events including G2/M transition, centrosome separation, and spindle formation [52][53]. Several members of NEK family of animals and a green alga *Chlamydomonas reinhardtii* regulate the disassembly of cilia and flagella [54]. Furthermore, *Aspergillus* NIMA, the founding member of NEKs, regulates directional cell growth through microtubule regulation in interphase [55], similar to the case of plant NEK members including *Arabidopsis* NEK6 [17] and *Marchantia polymorpha* MpNEK1 [19]. Because *Arabidopsis nek6* and *Marchantia* Mp*nek1* mutants do not exhibit any obvious phenotypic defects in mitosis, plant NEK members may have been co-opted to the mechanism of growth polarity during land plant evolution. It remains unclear whether animal and fungal NEKs also regulate microtubule response to mechanical stress to coordinate cellular and tissue growth.

A suboptimal response to mechanical stress buffers growth variations

Whether this is because of circadian rhythm, morphogen distribution or intrinsic stochasticity, growth is heterogeneous in time and space for most organisms [56][57][58]. This can generate local mechanical conflicts that are resolved either passively through large-scale tissue buckling or twisting (e.g. [59][60][61]), or actively used by the cells as an input to channel cell behavior [62]. For instance, in previous work, we found that meristematic cells overreact to such local conflicts to maintain a basal level of growth heterogeneity, and thus, to prime organogenesis [11]. Whereas mechanical forces may be viewed as factors adding robustness to morphogenesis, the analysis of *nek6* mutant now suggests that when the response to stress is too strong, shapes can also become variable and abnormal. This likely goes beyond NEK6, as past work showed that having hyper-aligned microtubules is not optimal for plant morphogenesis and growth (see e.g. [63][64]). In other words, the cell's response to mechanical stress needs to be suboptimal to promote developmental robustness. This result echoes plant-based computational simulations suggesting the ambivalent nature of mechanical stress in growth heterogeneity [11][65] and opens several avenues to test whether comparable conclusions can be reached in animal systems.

Acknowledgments

We thank Jan Traas and our colleagues for their comments and feedback on this manuscript, as well as Geoff Wasteneys for triggering this collaboration in 2014. This work was supported by the AgreenSkills+ fellowship program, which has received funding from the European Union's Seventh Framework Program under Grant Agreement FP7-609398 (AgreenSkills+ contract to ST), by Human Frontier Science Program Long-Term-Fellowship (LT000891/2018-L) to ST, by the European Research Council (ERC-2013-CoG-615739 ''MechanoDevo'') to OH, by Human Frontier Science Program grant RGP0023/2018 to OH, by JSPS KAKENHI Grants (16K07403 and 19K06709 to HM; 16J03501 to ST), by the NOVARTIS Foundation (Japan) for the Promotion of Science to HM, by the Okayama Foundation for Science and Technology to HM, and by Nakahara Education and Research Support Fund in Okayama University to HM.

Author contributions

S.T., S.V., and T.O. performed the experiments. S.T. analyzed the results. T. T., O.H. and H.M. supervised the work. S.T, O.H. and H.M. wrote the article.

Declaration of Interests

The authors declare no competing interests.

Figure legends

Figure 1. Amplified hypocotyl growth deviations in *nek6*

(A) Time lapse images of 2 to 3-day old wild type and *nek6-1* seedlings. (B) Time projections of the sequence shown in (A). (C) Quantification of hypocotyl waviness of wild-type (blue) and *nek6-1* (orange) hypocotyls. Waviness is the ratio of the length along hypocotyls and the shortest distance between the bottom and top of hypocotyls as shown in upper-right diagram. Waviness and length of each hypocotyl are plotted along the vertical and horizontal axes, respectively (Pearson's correlation; R_{WT} =0.34, P_{WT}=0.013, R_{nek6} =0.55, P_{nek6}=2.5x10^{-6}). (D-G) 3 to 4-day old etiolated wild-type and *nek6-1* seedlings exposed to gravistimulation (D,E) or mechanical friction (F,G). (D) Seedlings at 3 and 16 hours after gravistimulation. (E) Magnified images of seedlings at 20 hours after gravistimulation. (F) Vertically grown seedlings, as shown in the top diagram. (G) Seedlings grown on medium with an oblique orientation for 16 hours, as shown in the top diagram. (H and I) Quantification of waviness of hypocotyls after gravistimulation (H) or touch induction (I). Results are represented as box plots where "X" indicates mean value (* p<0.05, *** p<0.0001, Mann-Whitney U-test). Scale bars = 1 mm. See also Figure S1 and Video S1.

Figure 2. CMTs are hyper-aligned along the longitudinal axis of *nek6* hypocotyls in the fast-growing region

Time-course analysis of the CMT arrays was conducted in the rootward region of 2-day old hypocotyls over two hours. (A) Tracking of CMT arrays in wild-type and *nek6-1* hypocotyls for 2 hours. (B) Image overlay of cortical microtubules at 0 h (Cyan) and at 1 h (Red). Anisotropy and average orientation of the CMT arrays are quantified with FibrilTool and the results are represented by the length and orientation of the colored bars, respectively. (C and D) CMT array reorientation of individual cell over 1 hour (n_{WT}=136 cells from 13 hypocotyls, n_{nek6-1}=128 cells from 11 hypocotyls). (C) The Y axis indicates the CMT array orientation: 0°

correspond to a longitudinal orientation (i.e. parallel to the axis of the hypocotyl as shown by vectors in (B)). Colored lines connect values of CMT array orientation from the same cells at different time points (0h and 1h). 13 cells for which measured CMT reorientation was superior to 90 degrees were excluded from the analysis. (D) Quantification of CMT reorientation in each cell over 1 hour, as shown in (C). Results are represented as box plot where "X" indicates mean value (*** p<0.0001, Mann-Whitney U-test). Scale bars = 10 μm. See also Figure S2.

Figure 3. The CMT response to mechanical perturbations is more pronounced in *nek6*

(A) CMTs in wild type and *nek6-1* mutant at 0.5 hours and 2.5 hours after ablation. Anisotropy and average orientation of the CMT arrays are quantified with FibrilTool and the results are represented by the length and orientation of the colored bars, respectively. (B) Anisotropy of CMT arrays in cells surrounding the ablation site at 0.5h and at 2.5h after ablation. Data are represented as mean ± SEM (WT: n=93 cells from 11 hypocotyls, *nek6-1*: n=164 cells from 17 hypocotyls) (* p<0.05, ** p<0.001, *** p<0.0001, t-test). (C and D) Quantification of CMT orientation in cells surrounding the ablation site. (C) Close-up showing how CMT orientations were quantified (yellow angles). (D) Distribution of CMT orientations at 2.5 h after ablation (n_{WT}=93 cells from 11 hypocotyls, $n_{nek6\text{-}1}$=164 cells from 17 hypocotyls) (* p<0.05, Kolmogorov-Smirnov test). Scale bar = 50 μm. For the impact on growth, see Figure S3.

Figure 4. CMTs follow cell shape-derived stress pattern in slow growing region of *nek6-1* hypocotyls

CMTs are observed in the shootward cells of hypocotyls. (A) CMT arrays in 2-day old wild-type and *nek6-1* hypocotyls. An orthogonal section of the cells is presented to show the curvature of the outer wall. (B) Quantification of cell curvature along the length of 2-day old hypocotyls (n_{WT}=178 from 5 hypocotyls, $n_{nek6\text{-}1}$=165 from 5 hypocotyls). Curvature diameter is measured by fitting a circle on the outer wall, as shown in the upper-left diagram. Values from the cells with circumferential pattern are shown with red circle. Cell #1 is positioned at the bottom of the hypocotyl, as shown in Figure S2A. (C) Time-lapse images of CMTs in bulging cells in 3-day old *nek6-1* mutant before oryzalin treatment and up to 72 hours after washing out. (D) CMTs in 2-day old *nek6-1* mutant immediately and 1 hour after immersion in pure water. (E) Distribution of CMT array pattern types after immersion in water (n=93). (F) CMTs in 2-day old *nek6-1* mutant immediately and 1 hour after immersion in 0.2 M

mannitol solution. (G) Distribution of CMT array pattern types after immersion in 0.2 M mannitol (n=78). Scale bar =10 μm. For CMT patterns in older, bumpier, cells, see Figure S4.

Figure 5. The NEK6 protein exhibits a bipolar localization, with a bias on longitudinal microtubules, in young hypocotyls.

(A) NEK6 and microtubule distribution in a representative 2-day old hypocotyl. NEK6-GFP signal and microtubule (mCherry-TUB6) signal are colored in magenta and green, respectively. (B) Close-up on a cell from (A), marked with an asterisk, with merged and split channels: NEK6-GFP (left), mCherry-TUB6 (middle), merge (right). (C) Signal plot along the dotted yellow lines shown in (B) across the longitudinal and oblique microtubules. (D) Relative signal intensity of NEK6-GFP divided by the signal intensity of mCherry-TUB6 (n=156 from 16 cells from 4 hypocotyls). Microtubule orientation is measured for each microtubule as shown in the right diagram and is plotted on the horizontal axis. (E-I) Time-lapse imaging of NEK6-GFP and mCherrry-TUB6. Edgeward and centerward of kymograph is indicated by "e" and "c", respectively. (E) Close-up: NEK6-GFP and mCherry-TUB6 signal around cell edges. (F) Kymograph of NEK6-GFP signal in the region between two brackets in (E) in the time range from 0 sec to 297 sec. Yellow arrows indicate the onset of NEK6 migrations from the edge to the center. (G) Time-lapse images of NEK6-GFP and mCherry-TUB6 at the cell edge. Yellow arrows indicate the NEK6-GFP signals at the shrinking microtubule ends. (H) Image projection of NEK6-GFP from t=63 seconds to t=87 seconds including cell edge (dotted lines). Yellow arrow indicates the track of NEK6-GFP. (I) Kymograph of the NEK6-GFP and mCherry-TUB6 signals in the 71 sec to 102 sec timeframe along NEK6 trajectory shown in (H). (J) Proportion of fates of microtubule plus ends after interacting at the edge for 1 minute. The fates of microtubule plus ends are analyzed with respect to the presence or absence of NEK6-GFP signal (NEK6+/NEK6-), and are classified into four categories; bundle, pass, pause, shrink, see graphical explanations (Figure S5C - S5F) (n_{NEK6-}=153, n_{NEK6+}=193, *** p<0.0001, Fisher's exact test). Scale bar = 20 μm (A), 1 μm (G) (I), 2 μm (F), 5 μm (B) (E) (G) (H), 20 μm (A). Vertical scale bar = 60 sec (F), 20 sec (I). See also Figure S5 and video S2 and S3.

Figure 6. NEK6 preferentially localizes on CMTs that align with maximal tensile stress direction

(A) NEK6-GFP localization at 45 minutes and 160 minutes after ablation. (B) Close-up from panel (A) at t=160 min: NEK6-GFP signal (left), mCherry-TUB6 signal (middle) and merge

(right). A yellow line marks the proximo–distal path (p-d) for the NEK6-GFP signal plotted in (C). Scale bars = 20 μm. (C) Quantification of the NEK6 and microtubule signal intensity close (proximal) and away (distal) from the ablation site along the yellow line as shown in (B). (D) Quantification of relative intensity of NEK6-GFP divided by microtubule signal. Microtubule orientation around the ablation site is measured for each microtubule as shown in Figure 3C (n=130 CMTs in 23 cells from 5 hypocotyls; Pearson's correlation, r=0.36, $p=2.4x10^{-5}$). (E) Graphical abstract: NEK6-dependent depolymerization of microtubules aligning with maximal tensile stress buffers growth variation. See also Figure S6.

STAR methods

CONTACT FOR REAGENT AND RESOURCE SHARING

All plant lines are available for sharing. Further information and requests for resources and reagents should be directed to and will be fulfilled by the Lead Contact, Olivier Hamant (olivier.hamant@ens-lyon.fr) and Hiroyasu Motose (motose@cc.okayama-u.ac.jp).

EXPERIMENTAL MODEL AND SUBJECT DETAILS

Arabidopsis thaliana accession of Columbia-0 (used as the wild type), the *nek6-1* mutant (also called *ibo1-4*; [15] were used in this study. Surface sterilized seeds were sown on half-strength Murashige and Skoog agar medium (MS: Nihon Pharmaceutical, 1% agar: Sigma-Aldrich A1296, 1% sucrose, pH 5.8). Plants were incubated under a 16 h-light/8 h-dark photoperiod at 23°C. The microtubule markers *p35S::GFP-TUB6* [66] and *pUBQ10::mCherry-TUB6* [67], and the NEK6 microtubule double marker line *pNEK6::NEK6-GFP pUBQ10::mCherry-TUB6 / nek6-1* [17] were described previously.

METHOD DETAILS

Time-lapse observation of hypocotyl growth

For time-lapse observation, grooved agar medium was prepared by partially removing agar medium from the upper region of square agar plate. The 2-day old seedlings were transferred using tweezers so that seedlings attach agar only with their roots. This method prevents

hypocotyls and cotyledons from touching the agar medium. Touching stress severely affects growth and morphology of shoots. Time-lapse images were automatically taken by a SLR digital camera (D5600, Nikon, http://www.nikon.com) every hour under continuous light.

Quantification of the frequency of waviness and bends in hypocotyls

7-day old seedlings were imaged with a SLR digital camera (D5600, Nikon, http://www.nikon.com). Waviness and frequency of bends were analyzed with ImageJ. For waviness, hypocotyl length was divided by the straight distance between the top and bottom of the hypocotyl. Number of bends was counted using the segmented line (line tool of ImageJ). Segmented line was drawn along the central axis of hypocotyl with the constraint that the minimum number of segments should be drawn (i.e. segments should always be contained within the hypocotyl). The number of junctions between segments was counted as a proxy for the number of bends in the hypocotyl. The frequency of bends was calculated by dividing the number of junctions by the sum of the length of each segmented lines.

Gravistimulation and touch

In gravistimulation experiments, hypocotyls were grown in the dark without touching the agar medium by using the grooved agar method described above. Gravistimulation was induced by rotating agar plates by 90 degrees from the original orientation. To induce touch, the agar plates were inclined forward with an angle of 30 degrees from the horizontal plane to cause mechanical friction between the growing hypocotyls and the medium surface. Seedlings were grown in the dark throughout the experiment.

Microscopy

To image microtubules, the *nek6-1* mutant was crossed with the transgenic plants expressing *p35S::GFP-TUB6* or *pUBQ10::mCherry-TUB6*. When imaging at tissue scale, the *pUBQ10::mCherry-TUB6* line was used, as the *p35S::GFP-TUB6 nek6-1* exhibit mosaic expression. A complementation line of *pNEK6::NEK6-GFP pUBQ10::mCherry-TUB6 nek6-1* [17] was used to analyze NEK6 localization as well as microtubule organization. Microtubule and NEK6 behavior were imaged with a long-distance water dipping lens (x25, NA=0.95) using a Leica SP8 confocal microscope equipped with resonant scanner. During imaging, plants were kept on MS agar medium immersed in water (Hamant et al. 2008, Stanislas et al. 2017). To obtain surface signal of hypocotyl, z-stack images were processed using the ImageJ macro SurfCut [68]. Microtubule arrays were quantified with the ImageJ macro FibrilTool

[28]. Some images were also taken with other laser-scanning confocal microscopes, Zeiss LSM800 (Video S2) and Olympus FV1200 (Video S3). For time-lapse imaging, 2-day old, light grown, *pUBQ10::mCherry-TUB6* and *pNEK6::NEK6-GFP pUBQ10::mCherry-TUB6 nek6-1* seedlings were used to observe microtubule dynamics and NEK6 behavior during hypocotyl growth. The rootward region of the hypocotyl was imaged every hour using a Leica SP8 confocal microscope as described above. After imaging, plants were placed vertically in the normal growth condition, as described above, until the next imaging iteration.

Treatment with water or mannitol solution

MilliQ water (>18.5 MΩ) and 0.2 M mannitol solution were used to increase and decrease turgor pressure, respectively. 2-day old *p35S::GFP-TUB6* and *p35S::GFP-TUB6 nek6-1* seedlings were immersed in water or 0.2 M mannitol solution. Images were taken before and after the treatment using SP8 confocal microscopy (Leica) as described above. During image acquisition, 0.2 M mannitol solution was temporally replaced with water to obtain clear images. Image acquisition of all samples never took more than 15 minutes.

Microtubule repolymerization assay

During imaging, 3-day old *p35S::GFP-TUB6* and *p35S::GFP-TUB6 nek6-1* seedlings were immersed in water and held between glass slide and a cover slip throughout the observation. The gap between the slide and the cover slip was set at 0.5 to 1 mm with plastic tapes (822-2749, thickness 0.2 mm, ASKUL, Japan) to avoid pressing seedlings and to easily exchange liquids. To depolymerize cortical microtubules, water was replaced with 20 μM oryzalin solution for 3 hours. To repolymerize microtubules, oryzalin-treated seedlings were extensively washed five times by water. Hypocotyls were imaged by confocal microscopy (FV1200, Olympus) before and after treatment with oryzalin.

Cell ablation experiment

Hypocotyls of 2-day old *pUBQ10::mCherry-TUB6* and *pNEK6::NEK6-GFP pUBQ10::mCherry-TUB6 nek6-1* seedlings were used for ablation experiment. Ablations were performed manually with a fine needle (Minutien pin, 0.15 mm rod diameter, 0.02 mm tip width, RS-6083–15, Roboz Surgical Instrument Co.) under a stereomicroscope. Hypocotyls with ablated cells were imaged using SP8 confocal microscopy (Leica) as described above. Anisotropy and orientation of microtubule array were quantified using the ImageJ macro FibrilTool [28]. For the analysis of wound healing, z-stack images at two

different time points (2 to 2.4h and 4 to 4.5h) were first processed with an anisotropic filter [69] to obtain clear cell contours and then cell elongation was quantified with the MorphoGraphX plugin "Principal directions of growth (PDGs)" [70].

Quantification of relative NEK6 intensity and orientation of each microtubule

Microtubules around cell edge were randomly selected and lines were drawn along each microtubule by line tool in ImageJ. Intensities of both NEK6-GFP and mCherry-TUB6 were measured along each line. Line orientation was also measured at the same time. Relative NEK6-GFP signal intensity was calculated as the ratio of NEK6-GFP signal intensity over mCherry-TUB6 signal intensity for each line, and plotted with its angle.

QUANTITATIVE AND STATISTICAL ANALYSIS

Quantitative data were processed using Microsoft Excel software and statistical tests were conducted with R software. Statistical analysis of the results (sample size (n), *p*-value, type of test) is presented in the main text in the result section.

DATA AND CODE AVAILABILITY

This work does not involve the production of large datasets and uses published plugins or image analysis tools.

Supplemental video legends:

Video S1. Time-lapse movie of 2 to 3-day old wild type and *nek6-1* seedlings. Related to Figure 1 and S1. Wider view of time-lapse observation shown in Figure 1A. Scale bar = 1 mm

Video S2. Time-lapse movie of NEK6-GFP at cell edges. Related Figure 5E,F,J and S5C-S5G. Scale bar = 5 µm

Video S3. Time-lapse movie of NEK6-GFP at cell edges. Related Figure 5G,H,I. Scale bar = 5 µm

References

1. Goentoro, L., Shoval, O., Kirschner, M.W., and Alon, U. (2009). The Incoherent Feedforward Loop Can Provide Fold-Change Detection in Gene Regulation. Mol. Cell *36*, 894–899.
2. Davidson, L.A. (2017). Mechanical design in embryos: mechanical signalling, robustness and developmental defects. Philos. Trans. R. Soc. Lond. B. Biol. Sci. *372*.
3. Hamant, O., and Moulia, B. (2016). How do plants read their own shapes? New Phytol. *212*, 333–337.
4. Cosgrove, D.J. (2005). Growth of the plant cell wall. Nat. Rev. Mol. Cell Biol. *6*, 850–861.
5. Green, P., and King, A. (1966). A mechanism for the origin of specifically oriented textures in development with special reference to Nitella wall texture. Aust J Biol Sci, 421–437.
6. Hamant, O., Heisler, M.G., Jonsson, H., Krupinski, P., Uyttewaal, M., Bokov, P., Corson, F., Sahlin, P., Boudaoud, A., Meyerowitz, E.M., *et al.* (2008). Developmental patterning by mechanical signals in Arabidopsis. Science *322*, 1650–1655.
7. Sampathkumar, A., Krupinski, P., Wightman, R., Milani, P., Berquand, A., Boudaoud, A., Hamant, O., Jonsson, H., and Meyerowitz, E.M. (2014). Subcellular and supracellular mechanical stress prescribes cytoskeleton behavior in Arabidopsis cotyledon pavement cells. eLife *3*.
8. Robinson, S., and Kuhlemeier, C. (2018). Global Compression Reorients Cortical Microtubules in Arabidopsis Hypocotyl Epidermis and Promotes Growth. Curr. Biol. CB *28*, 1794–1802.e2.
9. Verger, S., Long, Y., Boudaoud, A., and Hamant, O. (2018). A tension-adhesion feedback loop in plant epidermis. eLife *7*.
10. Sapala, A., Runions, A., Routier-Kierzkowska, A.-L., Das Gupta, M., Hong, L., Hofhuis, H., Verger, S., Mosca, G., Li, C.-B., Hay, A., *et al.* (2018). Why plants make puzzle cells, and how their shape emerges. eLife *7*.
11. Uyttewaal, M., Burian, A., Alim, K., Landrein, B., Borowska-Wykret, D., Dedieu, A., Peaucelle, A., Ludynia, M., Traas, J., Boudaoud, A., *et al.* (2012). Mechanical stress acts via katanin to amplify differences in growth rate between adjacent cells in Arabidopsis. Cell *149*, 439–451.
12. Hervieux, N., Tsugawa, S., Fruleux, A., Dumond, M., Routier-Kierzkowska, A.-L., Komatsuzaki, T., Boudaoud, A., Larkin, J.C., Smith, R.S., Li, C.-B., *et al.* (2017). Mechanical Shielding of Rapidly Growing Cells Buffers Growth Heterogeneity and Contributes to Organ Shape Reproducibility. Curr. Biol. CB *27*, 3468–3479.e4.
13. Hervieux, N., Dumond, M., Sapala, A., Routier-Kierzkowska, A.-L., Kierzkowski, D., Roeder, A.H.K., Smith, R.S., Boudaoud, A., and Hamant, O. (2016). A Mechanical Feedback Restricts Sepal Growth and Shape in Arabidopsis. Curr. Biol. *26*, 1019–1028.
14. Bichet, A., Desnos, T., Turner, S., Grandjean, O., and Hofte, H. (2001). BOTERO1 is required for normal orientation of cortical microtubules and anisotropic cell expansion in Arabidopsis. Plant J. Cell Mol. Biol. *25*, 137–148.
15. Motose, H., Tominaga, R., Wada, T., Sugiyama, M., and Watanabe, Y. (2008). A NIMA-related protein kinase suppresses ectopic outgrowth of epidermal cells through its kinase activity and the association with microtubules. Plant J. Cell Mol. Biol. *54*, 829–844.
16. Motose, H., Hamada, T., Yoshimoto, K., Murata, T., Hasebe, M., Watanabe, Y., Hashimoto, T., Sakai, T., and Takahashi, T. (2011). NIMA-related kinases 6, 4, and 5 interact

with each other to regulate microtubule organization during epidermal cell expansion in Arabidopsis thaliana. Plant J. Cell Mol. Biol. *67*, 993–1005.
17. Takatani, S., Ozawa, S., Yagi, N., Hotta, T., Hashimoto, T., Takahashi, Y., Takahashi, T., and Motose, H. (2017). Directional cell expansion requires NIMA-related kinase 6 (NEK6)-mediated cortical microtubule destabilization. Sci. Rep. *7*, 7826.
18. Sakai, T., Honing, H. van der, Nishioka, M., Uehara, Y., Takahashi, M., Fujisawa, N., Saji, K., Seki, M., Shinozaki, K., Jones, M.A., *et al.* (2008). Armadillo repeat-containing kinesins and a NIMA-related kinase are required for epidermal-cell morphogenesis in Arabidopsis. Plant J. Cell Mol. Biol. *53*, 157–171.
19. Otani, K., Ishizaki, K., Nishihama, R., Takatani, S., Kohchi, T., Takahashi, T., and Motose, H. (2018). An evolutionarily conserved NIMA-related kinase directs rhizoid tip growth in the basal land plant Marchantia polymorpha. Dev. Camb. Engl. *145*.
20. Motose, H., Takatani, S., Ikeda, T., and Takahashi, T. (2012). NIMA-related kinases regulate directional cell growth and organ development through microtubule function in Arabidopsis thaliana. Plant Signal. Behav. *7*, 1552–1555.
21. Gendreau, E., Traas, J., Desnos, T., Grandjean, O., Caboche, M., and Höfte, H. (1997). Cellular basis of hypocotyl growth in Arabidopsis thaliana. Plant Physiol. *114*, 295–305.
22. Okada, K., and Shimura, Y. (1990). Reversible root tip rotation in Arabidopsis seedlings induced by obstacle-touching stimulus. Science *250*, 274–276.
23. Chan, J., Calder, G., Fox, S., and Lloyd, C. (2007). Cortical microtubule arrays undergo rotary movements in Arabidopsis hypocotyl epidermal cells. Nat. Cell Biol. *9*, 171–175.
24. Vineyard, L., Elliott, A., Dhingra, S., Lucas, J.R., and Shaw, S.L. (2013). Progressive transverse microtubule array organization in hormone-induced Arabidopsis hypocotyl cells. Plant Cell *25*, 662–676.
25. Baskin, T.I. (2005). Anisotropic expansion of the plant cell wall. Annu. Rev. Cell Dev. Biol. *21*, 203–222.
26. Crowell, E.F., Timpano, H., Desprez, T., Franssen-Verheijen, T., Emons, A.-M., Höfte, H., and Vernhettes, S. (2011). Differential regulation of cellulose orientation at the inner and outer face of epidermal cells in the Arabidopsis hypocotyl. Plant Cell *23*, 2592–2605.
27. Chan, J., Eder, M., Crowell, E.F., Hampson, J., Calder, G., and Lloyd, C. (2011). Microtubules and CESA tracks at the inner epidermal wall align independently of those on the outer wall of light-grown Arabidopsis hypocotyls. J. Cell Sci. *124*, 1088–1094.
28. Boudaoud, A., Burian, A., Borowska-Wykręt, D., Uyttewaal, M., Wrzalik, R., Kwiatkowska, D., and Hamant, O. (2014). FibrilTool, an ImageJ plug-in to quantify fibrillar structures in raw microscopy images. Nat. Protoc. *9*, 457–463.
29. Krupinski, P., Bozorg, B., Larsson, A., Pietra, S., Grebe, M., and Jönsson, H. (2016). A Model Analysis of Mechanisms for Radial Microtubular Patterns at Root Hair Initiation Sites. Front. Plant Sci. *7*, 1560.
30. Boudon, F., Chopard, J., Ali, O., Gilles, B., Hamant, O., Boudaoud, A., Traas, J., and Godin, C. (2015). A computational framework for 3D mechanical modeling of plant morphogenesis with cellular resolution. PLoS Comput. Biol. *11*.
31. Yu, M., Yuan, X., Lu, C., Le, S., Kawamura, R., Efremov, A.K., Zhao, Z., Kozlov, M.M., Sheetz, M., Bershadsky, A., *et al.* (2017). mDia1 senses both force and torque during F-actin filament polymerization. Nat. Commun. *8*, 1650.
32. Risca, V.I., Wang, E.B., Chaudhuri, O., Chia, J.J., Geissler, P.L., and Fletcher, D.A. (2012). Actin filament curvature biases branching direction. Proc. Natl. Acad. Sci. U. S. A. *109*, 2913–2918.

33. Riveline, D., Zamir, E., Balaban, N.Q., Schwarz, U.S., Ishizaki, T., Narumiya, S., Kam, Z., Geiger, B., and Bershadsky, A.D. (2001). Focal contacts as mechanosensors: externally applied local mechanical force induces growth of focal contacts by an mDia1-dependent and ROCK-independent mechanism. J. Cell Biol. *153*, 1175–1186.
34. Bertet, C., Sulak, L., and Lecuit, T. (2004). Myosin-dependent junction remodelling controls planar cell intercalation and axis elongation. Nature *429*, 667–671.
35. Sherrard, K., Robin, F., Lemaire, P., and Munro, E. (2010). Sequential activation of apical and basolateral contractility drives ascidian endoderm invagination. Curr. Biol. CB *20*, 1499–1510.
36. Vuong-Brender, T.T.K., Ben Amar, M., Pontabry, J., and Labouesse, M. (2017). The interplay of stiffness and force anisotropies drives embryo elongation. eLife *6*.
37. Landrein, B., and Hamant, O. (2013). How mechanical stress controls microtubule behavior and morphogenesis in plants: history, experiments and revisited theories. Plant J. Cell Mol. Biol. *75*, 324–338.
38. Bastien, R., Bohr, T., Moulia, B., and Douady, S. (2013). Unifying model of shoot gravitropism reveals proprioception as a central feature of posture control in plants. Proc. Natl. Acad. Sci. U. S. A. *110*, 755–760.
39. Ikushima, T., and Shimmen, T. (2005). Mechano-sensitive orientation of cortical microtubules during gravitropism in azuki bean epicotyls. J. Plant Res. *118*, 19–26.
40. Zandomeni, K., and Schopfer, P. (1994). Mechanosensory microtubule reorientation in the epidermis of maize coleoptiles subjected to bending stress. Protoplasma *182*, 96–101.
41. Fischer, K., and Schopfer, P. (1997). Interaction of auxin, light, and mechanical stress in orienting microtubules in relation to tropic curvature in the epidermis of maize coleoptiles. Protoplasma *196*, 108–116.
42. Hamant, O., Inoue, D., Bouchez, D., Dumais, J., and Mjolsness, E. (2019). Are microtubules tension sensors? Nat. Commun. *10*, 2360.
43. Díaz-Valencia, J.D., Morelli, M.M., Bailey, M., Zhang, D., Sharp, D.J., and Ross, J.L. (2011). Drosophila Katanin-60 Depolymerizes and Severs at Microtubule Defects. Biophys. J. *100*, 2440–2449.
44. Takatani, S., Otani, K., Kanazawa, M., Takahashi, T., and Motose, H. (2015). Structure, function, and evolution of plant NIMA-related kinases: implication for phosphorylation-dependent microtubule regulation. J. Plant Res. *128*, 875–891.
45. Adamowski, M., Li, L., and Friml, J. (2019). Reorientation of Cortical Microtubule Arrays in the Hypocotyl of Arabidopsis thaliana Is Induced by the Cell Growth Process and Independent of Auxin Signaling. Int. J. Mol. Sci. *20*, 3337.
46. Elliott, A., and Shaw, S.L. (2018). Microtubule Array Patterns Have a Common Underlying Architecture in Hypocotyl Cells. Plant Physiol. *176*, 307–325.
47. Thoms, D., Vineyard, L., Elliott, A., and Shaw, S.L. (2018). CLASP Facilitates Transitions between Cortical Microtubule Array Patterns. Plant Physiol. *178*, 1551–1567.
48. Ambrose, C., Allard, J.F., Cytrynbaum, E.N., and Wasteneys, G.O. (2011). A CLASP-modulated cell edge barrier mechanism drives cell-wide cortical microtubule organization in Arabidopsis. Nat. Commun. *2*, 430.
49. Nakamura, M., Lindeboom, J.J., Saltini, M., Mulder, B.M., and Ehrhardt, D.W. (2018). SPR2 protects minus ends to promote severing and reorientation of plant cortical microtubule arrays. J. Cell Biol. *217*, 915–927.
50. Fan, Y., Burkart, G.M., and Dixit, R. (2018). The Arabidopsis SPIRAL2 Protein Targets and Stabilizes Microtubule Minus Ends. Curr. Biol. CB *28*, 987–994.e3.

51. Wightman, R., Chomicki, G., Kumar, M., Carr, P., and Turner, S.R. (2013). SPIRAL2 determines plant microtubule organization by modulating microtubule severing. Curr. Biol. CB *23*, 1902–1907.
52. O'Connell, M.J., Krien, M.J.E., and Hunter, T. (2003). Never say never. The NIMA-related protein kinases in mitotic control. Trends Cell Biol. *13*, 221–228.
53. Fry, A.M., O'Regan, L., Sabir, S.R., and Bayliss, R. (2012). Cell cycle regulation by the NEK family of protein kinases. J. Cell Sci. *125*, 4423–4433.
54. Quarmby, L.M., and Mahjoub, M.R. (2005). Caught Nek-ing: cilia and centrioles. J. Cell Sci. *118*, 5161–5169.
55. Govindaraghavan, M., McGuire Anglin, S.L., Shen, K.-F., Shukla, N., De Souza, C.P., and Osmani, S.A. (2014). Identification of interphase functions for the NIMA kinase involving microtubules and the ESCRT pathway. PLoS Genet. *10*, e1004248.
56. Mestek Boukhibar, L., and Barkoulas, M. (2016). The developmental genetics of biological robustness. Ann. Bot. *117*, 699–707.
57. Tsimring, L.S. (2014). Noise in biology. Rep. Prog. Phys. Phys. Soc. G. B. *77*, 026601.
58. Hong, L., Dumond, M., Zhu, M., Tsugawa, S., Li, C.-B., Boudaoud, A., Hamant, O., and Roeder, A.H.K. (2018). Heterogeneity and Robustness in Plant Morphogenesis: From Cells to Organs. Annu. Rev. Plant Biol. *69*, 469–495.
59. Coen, E., and Rebocho, A.B. (2016). Resolving Conflicts: Modeling Genetic Control of Plant Morphogenesis. Dev. Cell *38*, 579–583.
60. Wada, H., and Matsumoto, D. (2018). Twisting Growth in Plant Roots. In Plant Biomechanics, A. Geitmann and J. Gril, eds. (Cham: Springer International Publishing), pp. 127–140. Available at: http://link.springer.com/10.1007/978-3-319-79099-2_6 [Accessed November 17, 2018].
61. Verger, S., Liu, M., and Hamant, O. (2019). Mechanical Conflicts in Twisting Growth Revealed by Cell-Cell Adhesion Defects. Front. Plant Sci. *10*. Available at: https://www.frontiersin.org/article/10.3389/fpls.2019.00173/full [Accessed March 11, 2019].
62. Lecuit, T., and Lenne, P.-F. (2007). Cell surface mechanics and the control of cell shape, tissue patterns and morphogenesis. Nat. Rev. Mol. Cell Biol. *8*, 633–644.
63. Ambrose, J.C., and Wasteneys, G.O. (2008). CLASP modulates microtubule-cortex interaction during self-organization of acentrosomal microtubules. Mol. Biol. Cell *19*, 4730–4737.
64. Kong, Z., Hotta, T., Lee, Y.-R.J., Horio, T., and Liu, B. (2010). The γ -Tubulin Complex Protein GCP4 Is Required for Organizing Functional Microtubule Arrays in *Arabidopsis thaliana*. Plant Cell *22*, 191–204.
65. Fruleux, A., and Boudaoud, A. (2019). Modulation of tissue growth heterogeneity by responses to mechanical stress. Proc. Natl. Acad. Sci., 201815342.
66. Nakamura, M., Naoi, K., Shoji, T., and Hashimoto, T. (2004). Low concentrations of propyzamide and oryzalin alter microtubule dynamics in Arabidopsis epidermal cells. Plant Cell Physiol. *45*, 1330–1334.
67. Fujita, S., Pytela, J., Hotta, T., Kato, T., Hamada, T., Akamatsu, R., Ishida, Y., Kutsuna, N., Hasezawa, S., Nomura, Y., *et al.* (2013). An atypical tubulin kinase mediates stress-induced microtubule depolymerization in Arabidopsis. Curr. Biol. CB *23*, 1969–1978.
68. Erguvan, Ö., Louveaux, M., Hamant, O., and Verger, S. (2019). ImageJ SurfCut: a user-friendly pipeline for high-throughput extraction of cell contours from 3D image stacks. BMC Biol. *17*, 38.

69. Kiss, A., Moreau, T., Mirabet, V., Calugaru, C.I., Boudaoud, A., and Das, P. (2017). Segmentation of 3D images of plant tissues at multiple scales using the level set method. Plant Methods *13*, 114.
70. Barbier de Reuille, P., Routier-Kierzkowska, A.-L., Kierzkowski, D., Bassel, G.W., Schüpbach, T., Tauriello, G., Bajpai, N., Strauss, S., Weber, A., Kiss, A., *et al.* (2015). MorphoGraphX: A platform for quantifying morphogenesis in 4D. eLife *4*, 05864.

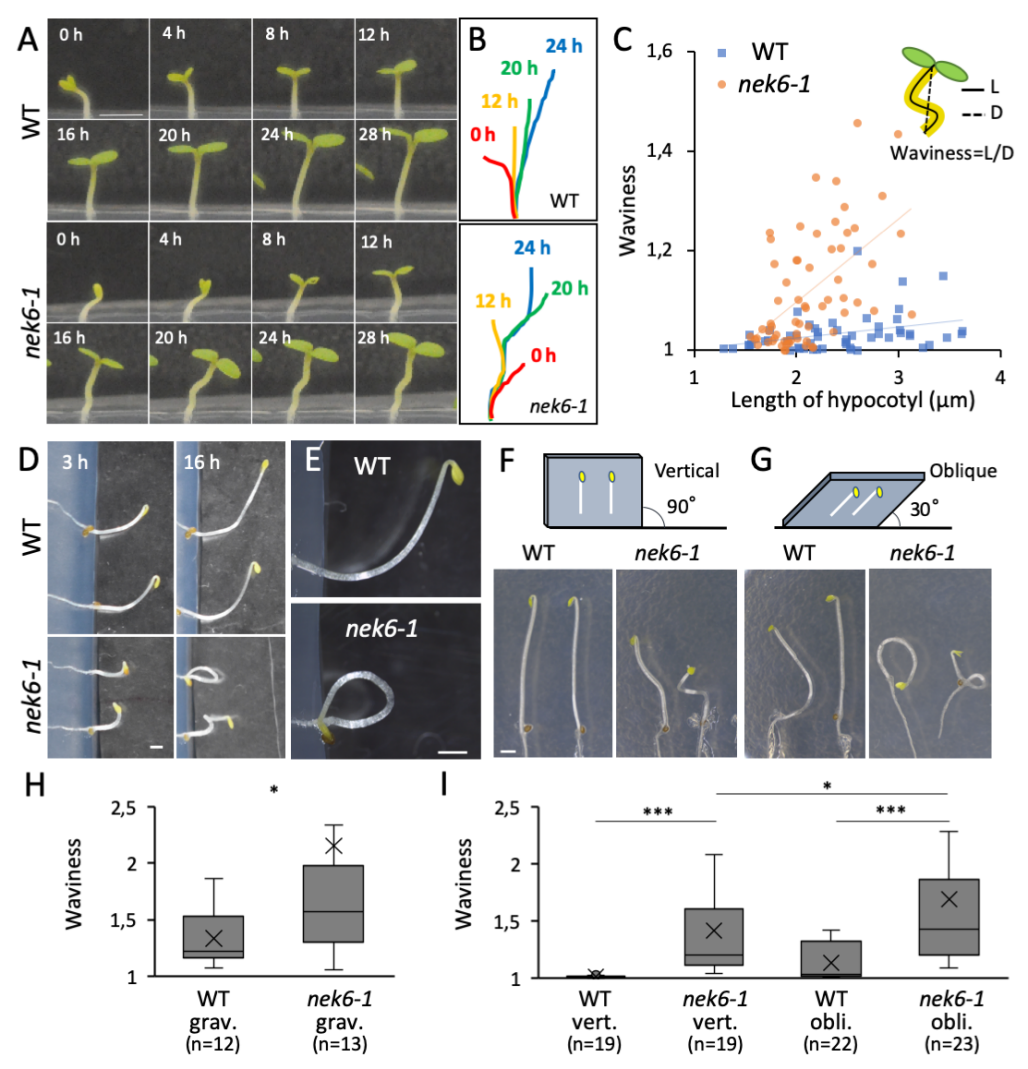
A
0 h
4 h
8 h
12 h
WT
16 h
20 h
24 h
28 h
nek6-1
B
24 h
20 h
12 h
0 h
WT
nek6-1
C
WT
nek6-1
L
D
Waviness=L/D
Waviness
Length of hypocotyl (µm)
D
3 h
16 h
E
F
Vertical
90°
G
Oblique
30°
H
Waviness
WT grav. (n=12)
nek6-1 grav. (n=13)
I
WT vert. (n=19)
nek6-1 vert. (n=19)
WT obli. (n=22)
nek6-1 obli. (n=23)

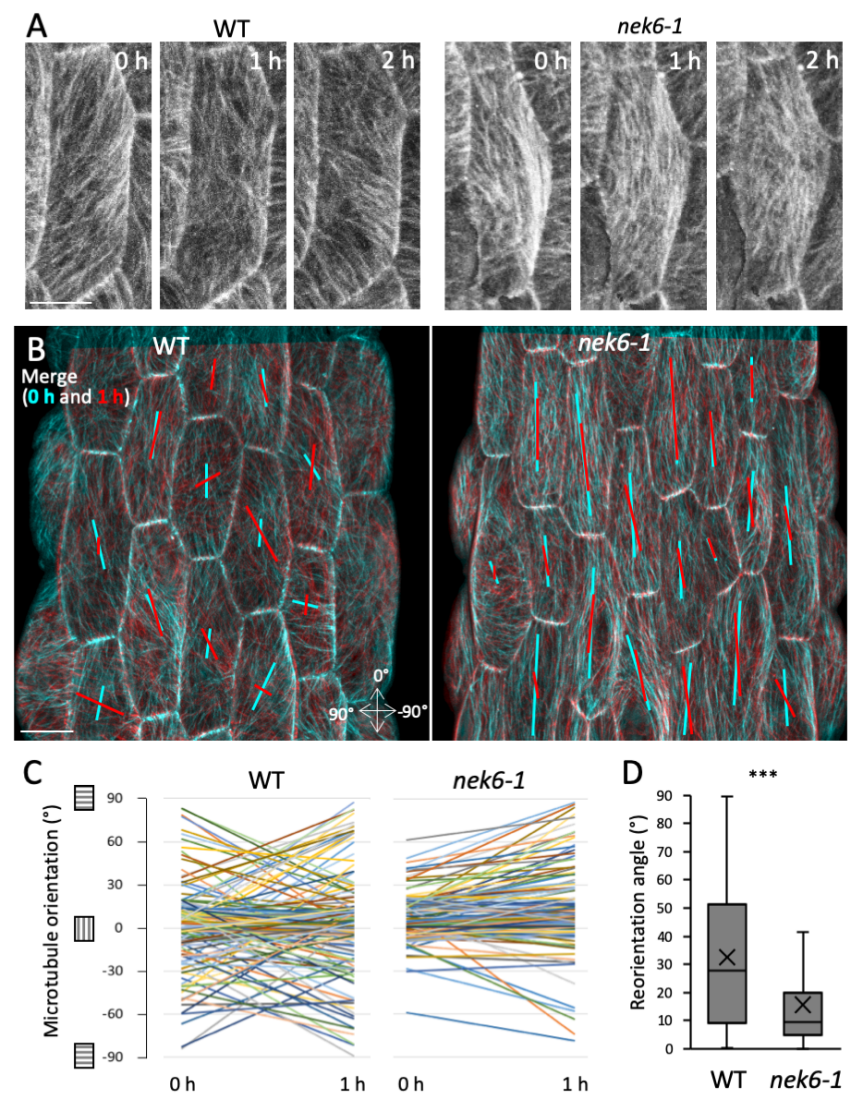
A
WT
nek6-1
0 h
1 h
2 h
0 h
1 h
2 h
B
WT
nek6-1
Merge
(0 h and 1 h)
0°
90°
-90°
C
WT
nek6-1
Microtubule orientation (°)
90
60
30
0
-30
-60
-90
0 h
1 h
0 h
1 h
D
***
Reorientation angle (°)
90
80
70
60
50
40
30
20
10
0
WT
nek6-1

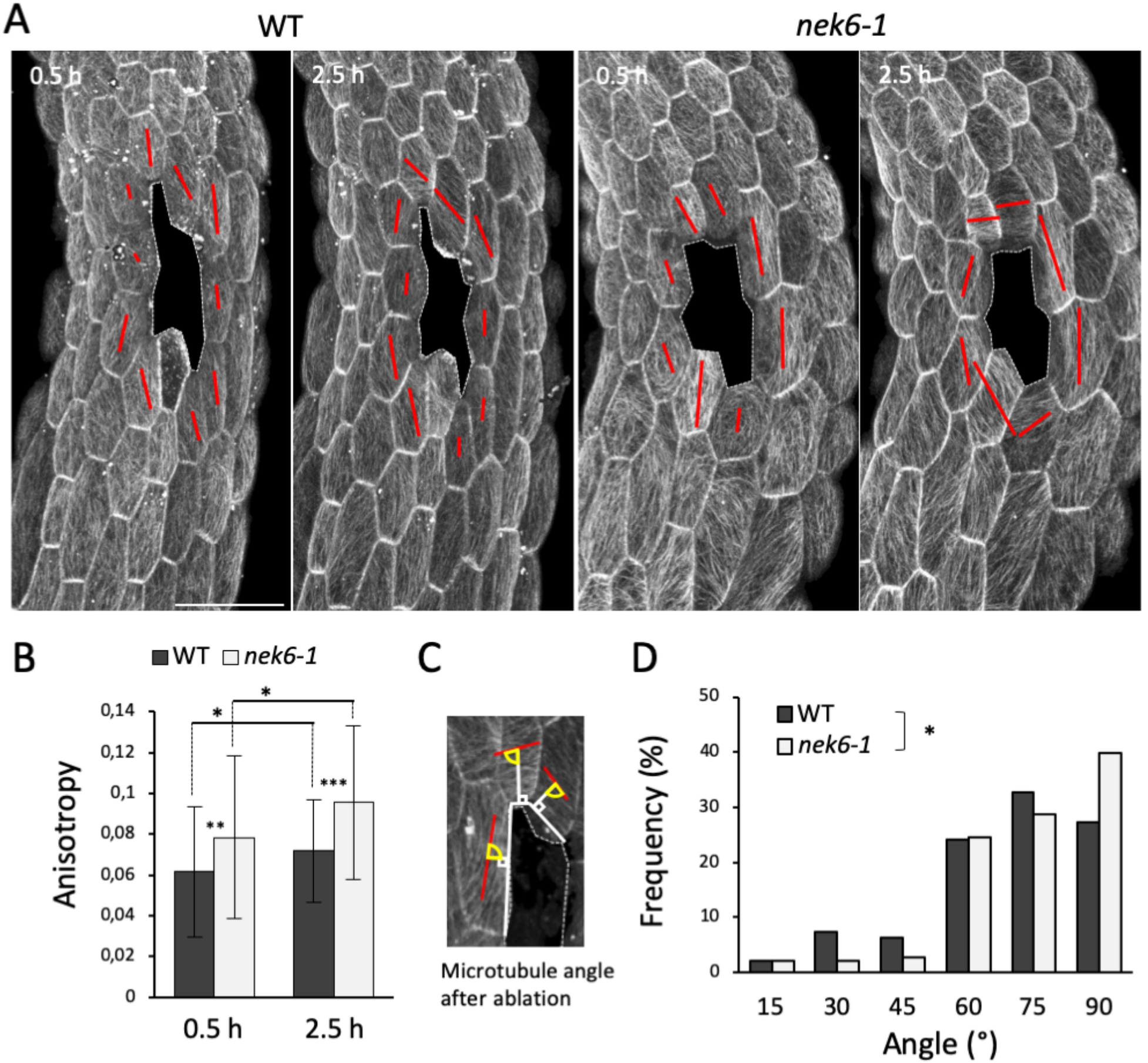
A
WT
nek6-1
0.5 h
2.5 h
0.5 h
2.5 h
B
WT
nek6-1
Anisotropy
0,14
0,12
0,1
0,08
0,06
0,04
0,02
0
*
*
**
***
0.5 h
2.5 h
C
Microtubule angle
after ablation
D
WT
nek6-1
*
Frequency (%)
50
40
30
20
10
0
15
30
45
60
75
90
Angle (°)

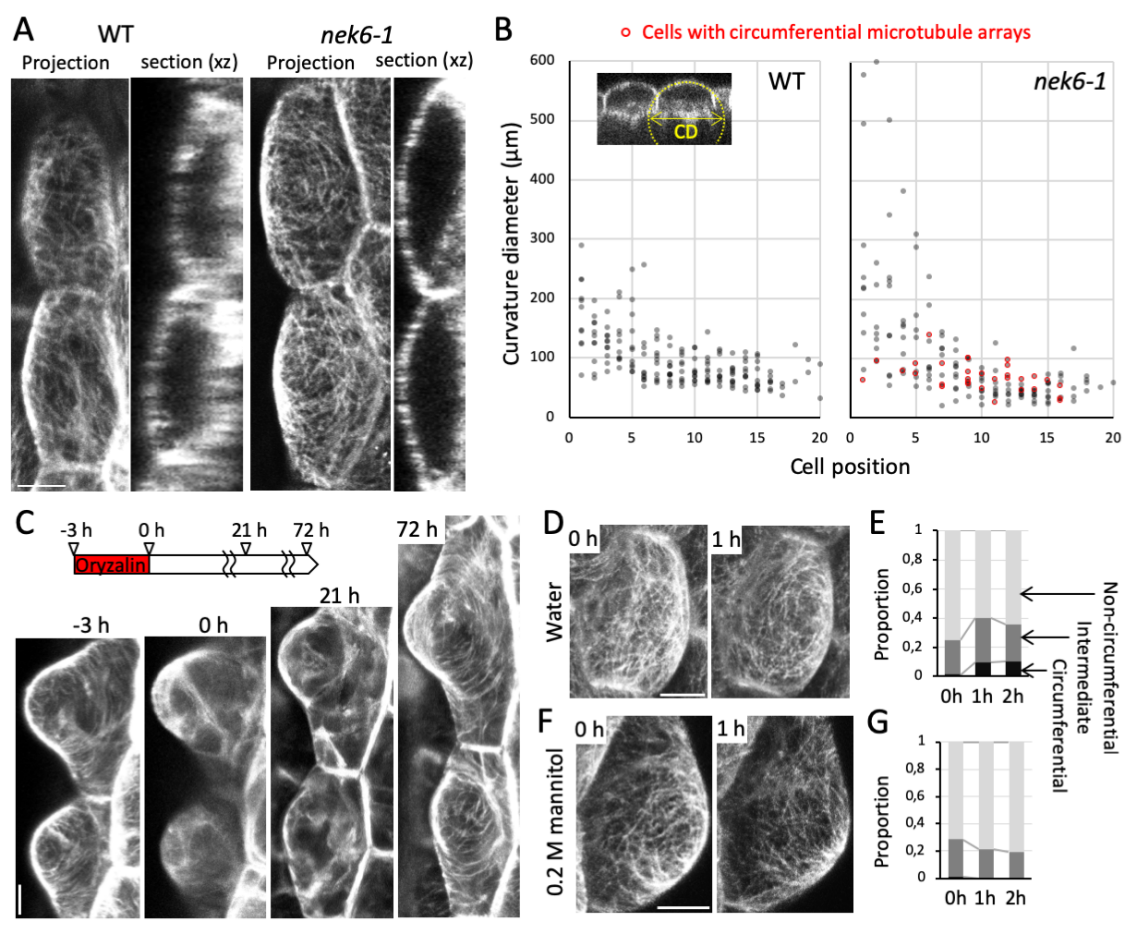
A
WT
nek6-1
Projection
section (xz)
Projection
section (xz)
B
Cells with circumferential microtubule arrays
WT
nek6-1
CD
Curvature diameter (µm)
Cell position
C
-3 h
0 h
21 h
72 h
Oryzalin
72 h
21 h
-3 h
0 h
D
0 h
1 h
Water
E
Proportion
Non-circumferential
Intermediate
Circumferential
0h 1h 2h
F
0 h
1 h
0.2 M mannitol
G
Proportion
0h 1h 2h

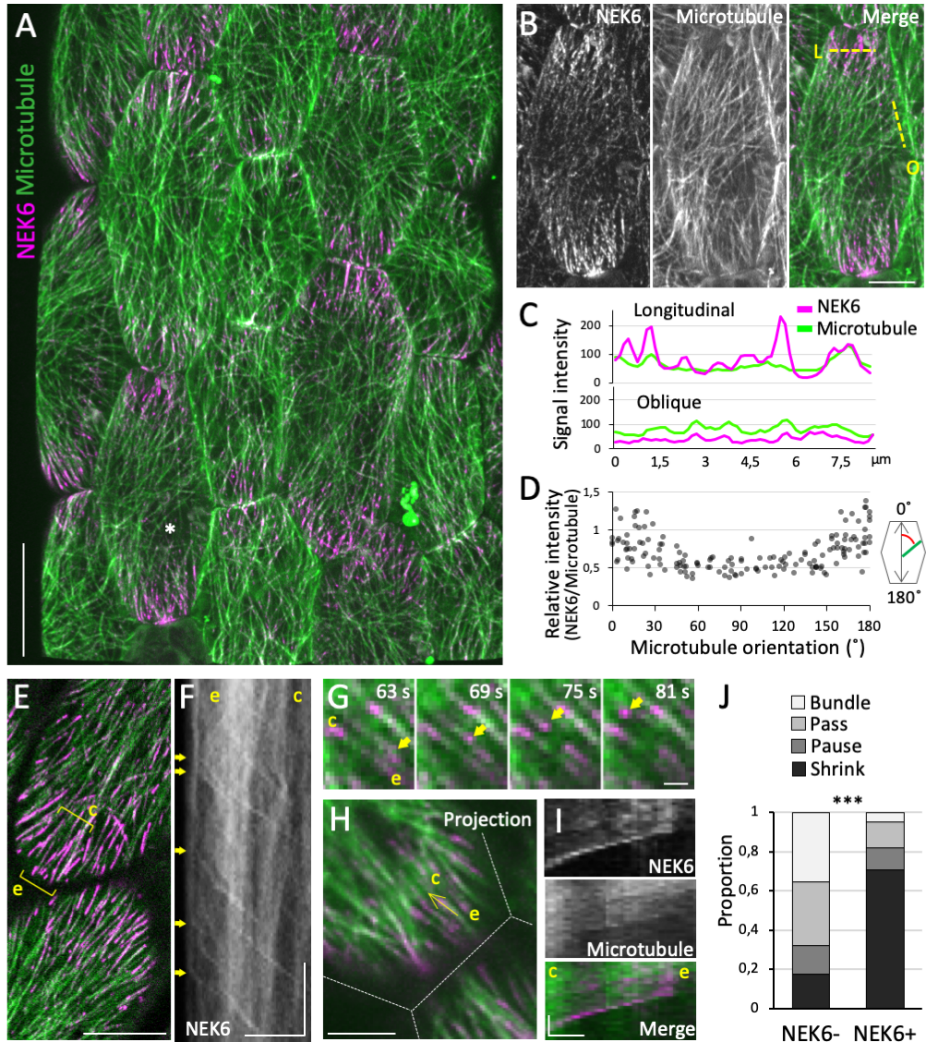
A
NEK6 Microtubule
*
B
NEK6
Microtubule
Merge
L
O
C
Longitudinal
Oblique
NEK6
Microtubule
Signal intensity
200
100
0
0
1,5
3
4,5
6
7,5
µm
D
Relative intensity (NEK6/Microtubule)
1,5
1
0,5
0
0
30
60
90
120
150
180
Microtubule orientation (°)
0°
180°
E
c
e
F
e
c
NEK6
G
63 s
69 s
75 s
81 s
c
e
H
Projection
c
e
I
NEK6
Microtubule
c
e
Merge
J
Bundle
Pass
Pause
Shrink
***
Proportion
1
0,8
0,6
0,4
0,2
0
NEK6-
NEK6+

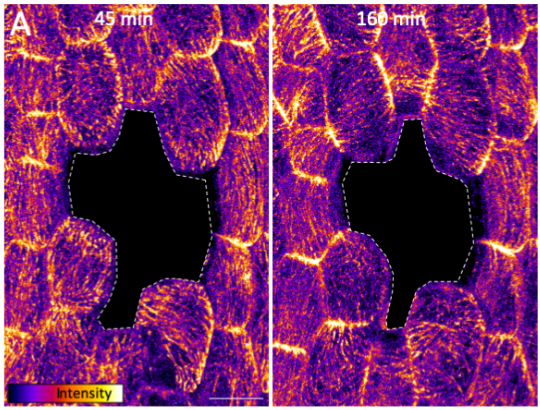
A
45 min
160 min
Intensity

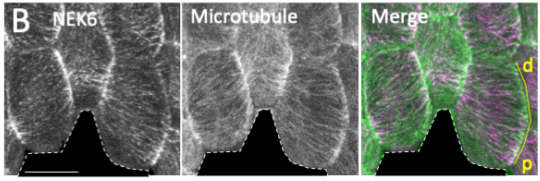
B
NEK6
Microtubule
Merge
d
p

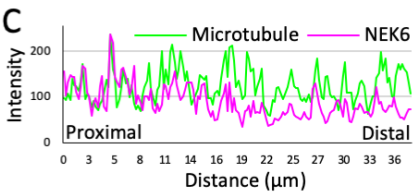
C
Microtubule
NEK6
Intensity
200
100
0
Proximal
Distal
0 3 5 8 11 14 16 19 22 25 27 30 33 36
Distance (µm)

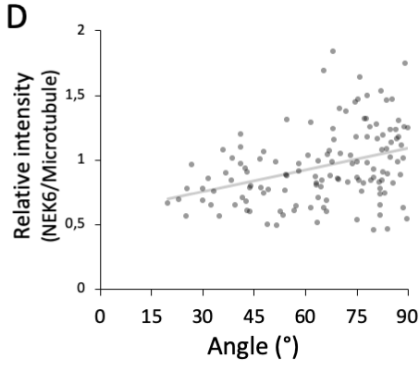
D
Relative intensity
(NEK6/Microtubule)
2
1,5
1
0,5
0
0 15 30 45 60 75 90
Angle (°)

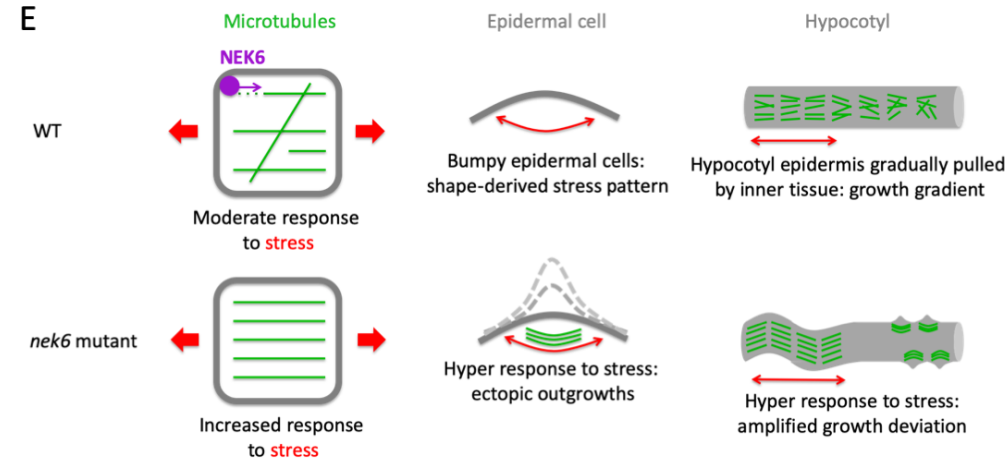
E
Microtubules
Epidermal cell
Hypocotyl
NEK6
WT
Moderate response
to stress
Bumpy epidermal cells:
shape-derived stress pattern
Hypocotyl epidermis gradually pulled
by inner tissue: growth gradient
nek6 mutant
Increased response
to stress
Hyper response to stress:
ectopic outgrowths
Hyper response to stress:
amplified growth deviation

Hypocotyl

Microtubules

WT

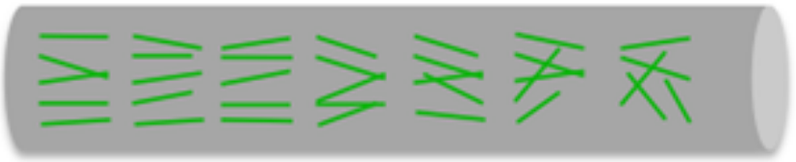

Growth averaging &
reduced proprioception

NEK6

Moderate response
to stress

nek6

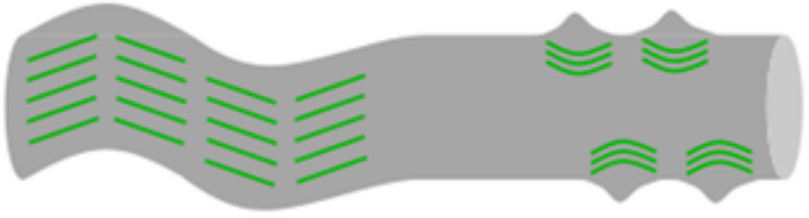

Amplified
growth deviation

Enhanced response
to stress